

## Electronic Supplementary Information (ESI)

### **CaH<sub>2</sub>-assisted low temperature synthesis of metallic magnetic nanoparticle-loaded multiwalled carbon nanotubes**

Liis Seinberg<sup>a</sup>, Shinpei Yamamoto<sup>\*,b</sup>, Masahiko Tsujimoto<sup>b</sup>, Yoji Kobayashi<sup>a</sup>, Mikio Takano<sup>b</sup> and Hiroshi Kageyama<sup>a,b,c</sup>

<sup>a</sup> *Department of Energy and Hydrocarbon Chemistry, Graduate School of Engineering, Kyoto University, Nishikyo-ku, Kyoto, 615-8510, Japan.*

<sup>\*,b</sup> *Institute for Integrated Cell-Material Sciences, Kyoto University, Yoshida-Ushinomiya-cho, Sakyo-ku, Kyoto, 606-8501, Japan. FAX: +81-75-383-2510; TEL: + 81-75-383-2513; E-mail: [yamamoto@icems.kyoto-u.ac.jp](mailto:yamamoto@icems.kyoto-u.ac.jp)*

<sup>c</sup> *CREST, Japan Science and Technology Agency (JST)*

## Experimental Section

### Synthesis of Fe or Ni NP-loaded MWCNTs

The reduction with CaH<sub>2</sub> was carried out following the method described elsewhere.<sup>1,2</sup> Briefly, nickel(II) stearate (Ni(SA)<sub>2</sub>, Mitsuwa Chemicals, 99 %), or iron stearate (Fe(SA)<sub>3</sub>, Mitsuwa Chemicals, 99 %), and one-weight excess of CaH<sub>2</sub> (Aldrich, 95 %) were finely ground in a N<sub>2</sub>-filled glove box and sealed in an evacuated Pyrex tube (length of ~15 cm and inner diameter of 6 mm). The tubes were inserted into furnace at room temperature and heated up to certain temperatures (300, 350, 400, 450 and 500 °C) at a rate of 300 °C/hr and kept for 24 hrs or 240 hrs depending on the experiment. Byproducts such as CaO produced during the reduction and residual CaH<sub>2</sub> were removed by washing with a 0.3 M methanol solution of NH<sub>4</sub>Cl (Wako, 99.5%) under constant sonication for 15 minutes; the process was repeated twice, followed by washing with methanol for several times in open air.

### Characterization Methods

Low- and high-magnification transmission electron microscopic (TEM) observations were performed by using JEOL JEM 1400D and 2200FS, respectively. TEM samples were prepared by dropping methanol solution containing the sample on Cu grid. Powder X-ray Diffraction (XRD) measurements were performed with Bruker D8 operating with Cu K $\alpha$  radiation ( $\lambda = 0.154$  nm) with 40 kV beam voltage and 40 mA beam current. Patterns were collected in a range from 15 ° to 85 ° with the steps of 0.04° and the exposure time of 4 sec. Thermogravimetric (TG) analyses were performed using a TG-DTA2000SA (Bruker AXS). All the TG measurements were performed using alumina pans and  $\alpha$ -Al<sub>2</sub>O<sub>3</sub> as a reference. The measurements were performed by heating the sample up to 700 °C (10 °C/min) and kept for 2 hrs under oxygen gas flow (100 mL/min). Weight fraction of the magnetic element (Ni or Fe) in the sample was calculated from the weight of the final oxidized products ( $\alpha$ -Fe<sub>2</sub>O<sub>3</sub> or NiO). Magnetic properties were characterized by using a Physical Properties Measurement System (Quantum Design PPMS-9RST) with a vibrating sample magnetometer (VSM) attachment. Raman spectra were collected by using a LabRAM HR800 (HORIBA Jobin Yvon Ltd.) with a semiconductor laser at 488 nm and at room temperature. <sup>1</sup>H-NMR measurement was performed by using an AVANCHE III NMR spectrometer (Bruker Biospin). For the NMR measurement, fragments were extracted from the crude mixture by using CHCl<sub>3</sub>.

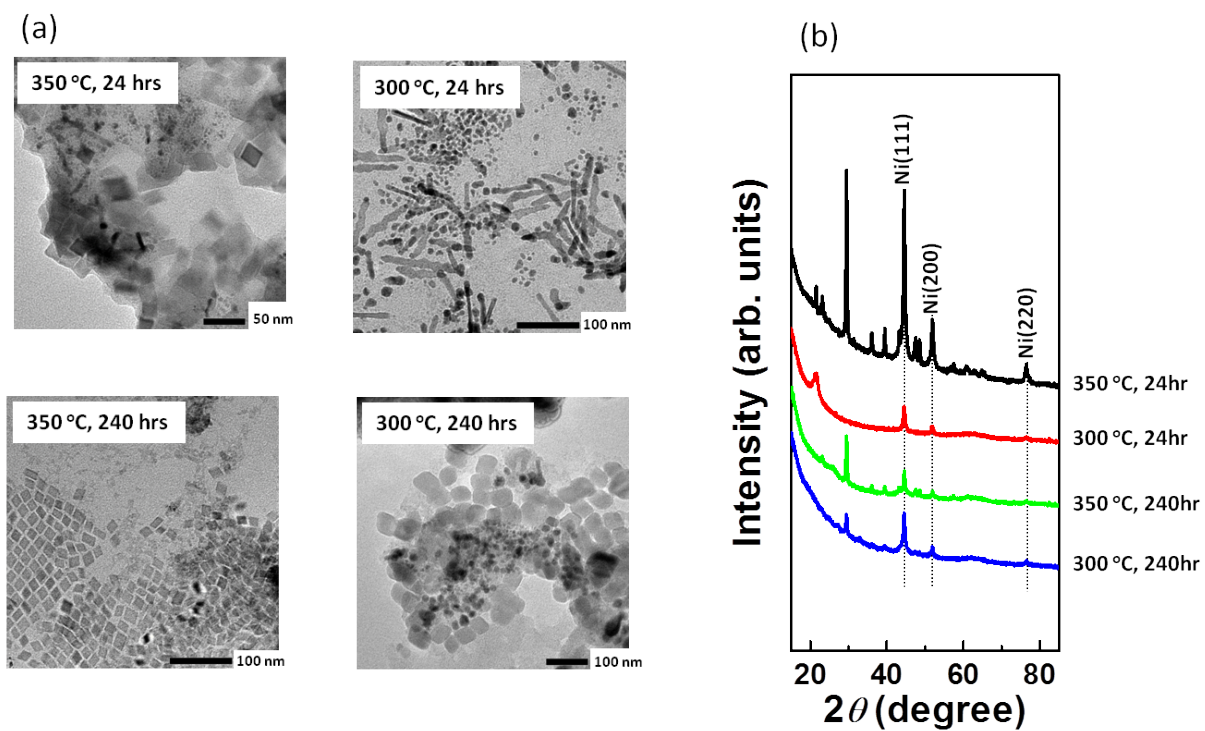


**Figure S1.** (a) TEM images and (b) XRD patterns of the samples prepared with Ni(SA)<sub>2</sub> at lower temperatures. No MWCNTs as well as graphitic peaks were observed. Note that rod-like objects observed in the TEM image (300 °C, 24 hr) are not MWCNTs although details are not clear at present.

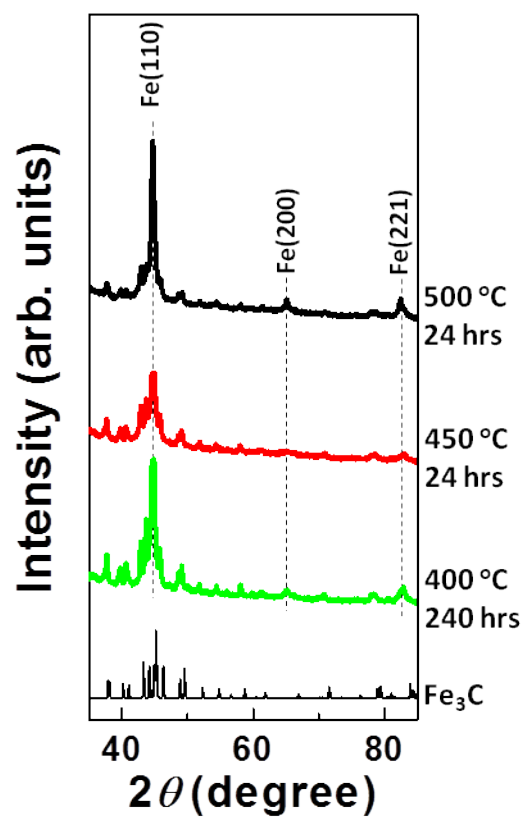


**Figure S2.** XRD patterns of the samples prepared with  $\text{Fe}(\text{SA})_3$  and a typical XRD pattern of  $\text{Fe}_3\text{C}$  (ICSD #167344).

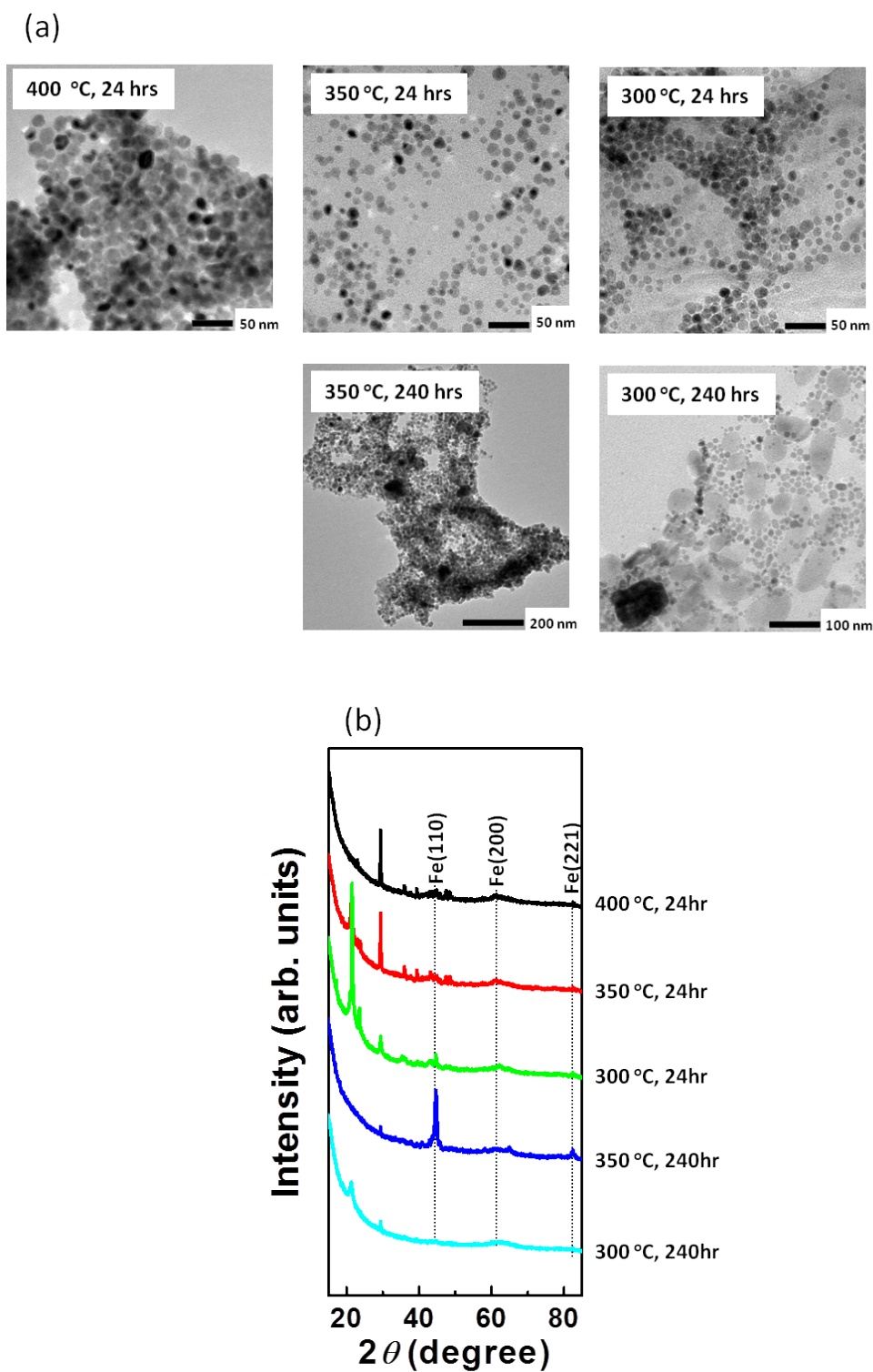


**Figure S3.** (a) TEM images and (b) XRD patterns of the samples prepared with  $\text{Fe}(\text{SA})_3$  at lower temperatures. No MWCNTs as well as graphitic peaks were observed.

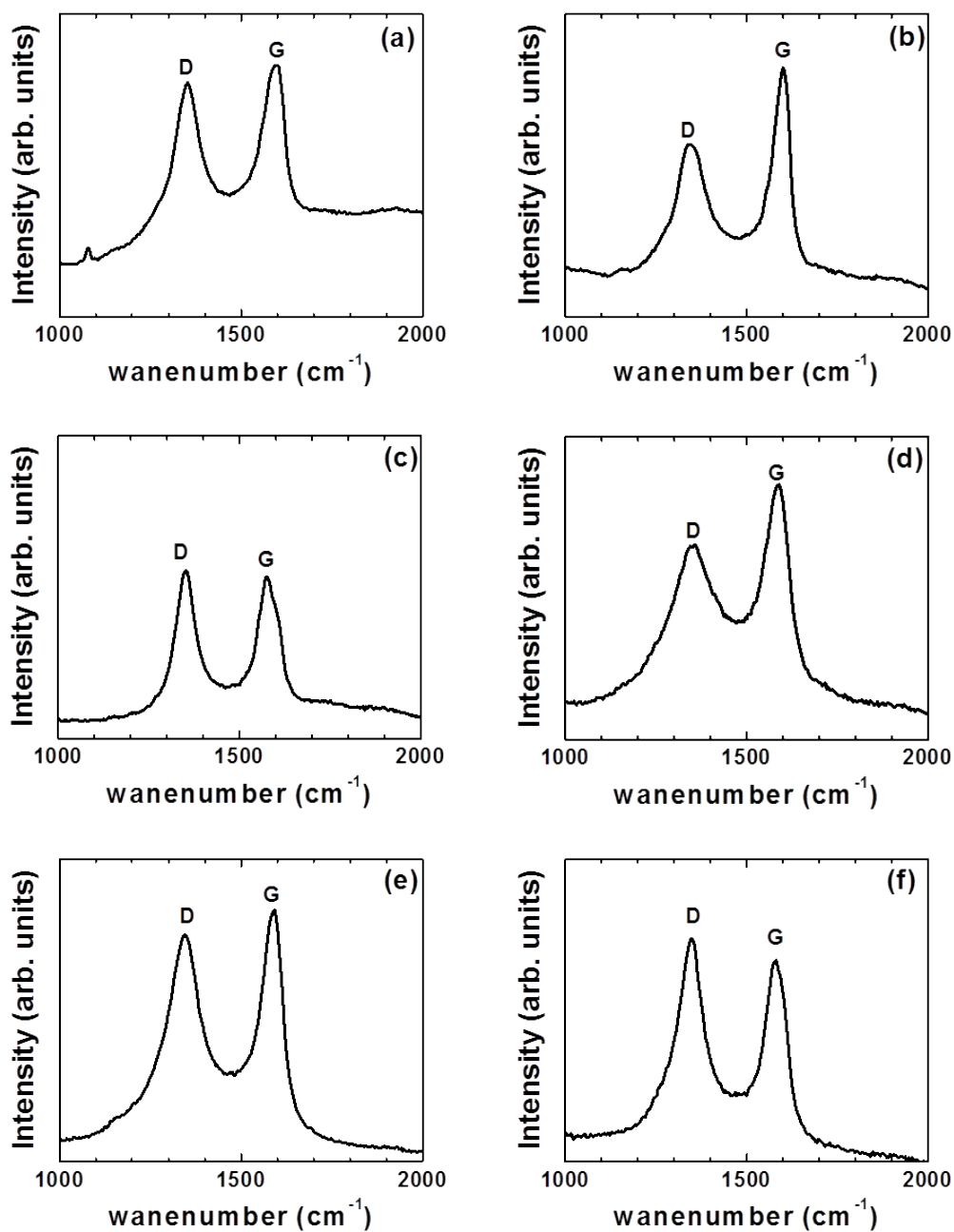


**Figure S4.** Raman spectra of the samples prepared with Ni(SA)<sub>2</sub> at (a) 400 °C, (b) 450 °C and (c) 500 °C for 24 hrs and with Fe(SA)<sub>3</sub> at (d) 400 °C for 240 hrs, (e) 450 °C for 24 hrs and (f) 500 °C for 24 hrs.

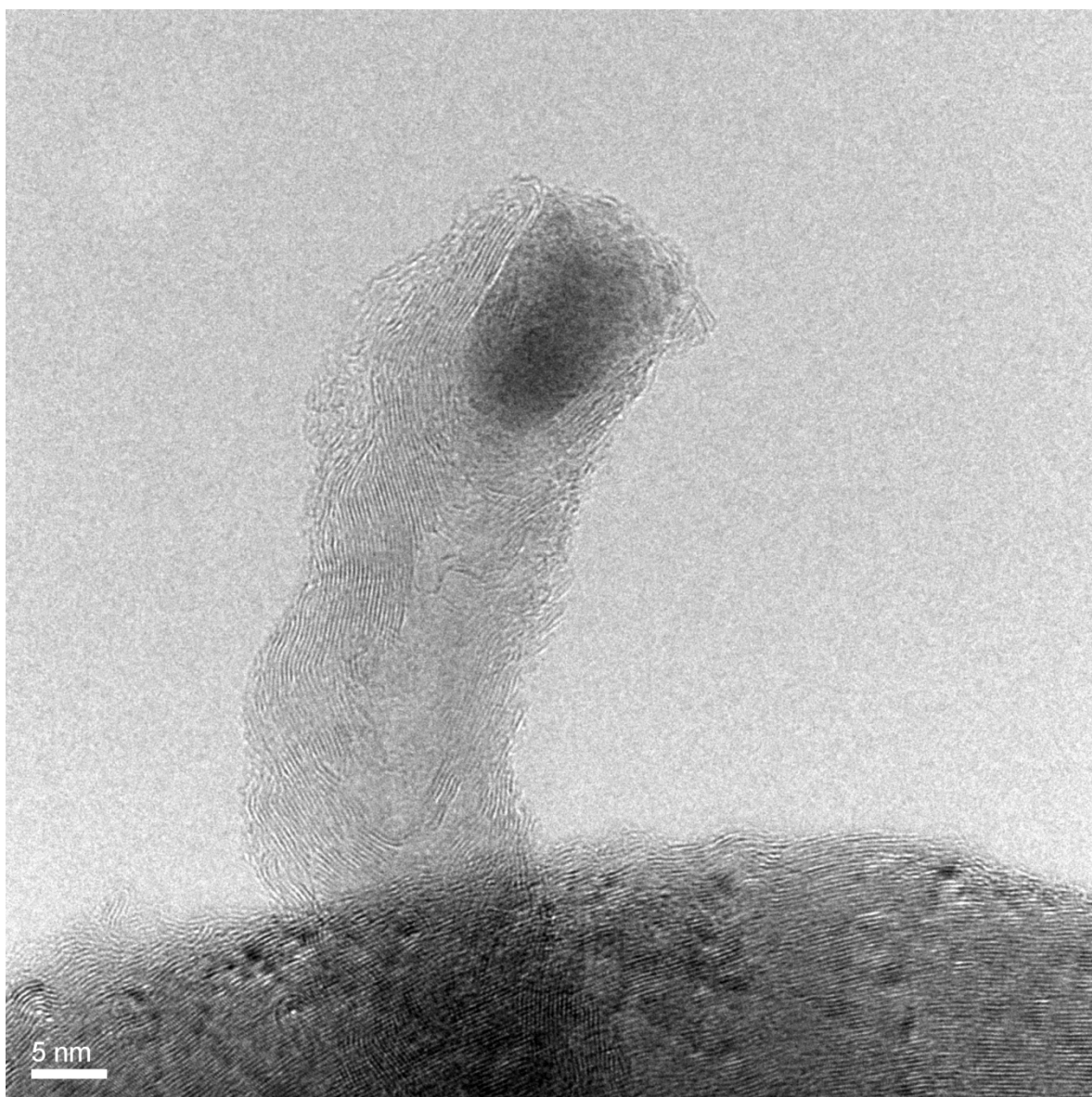


**Figure S5.** Typical high magnification TEM image of the sample prepared with Ni(SA)<sub>2</sub> at 500 °C for 24 hrs.

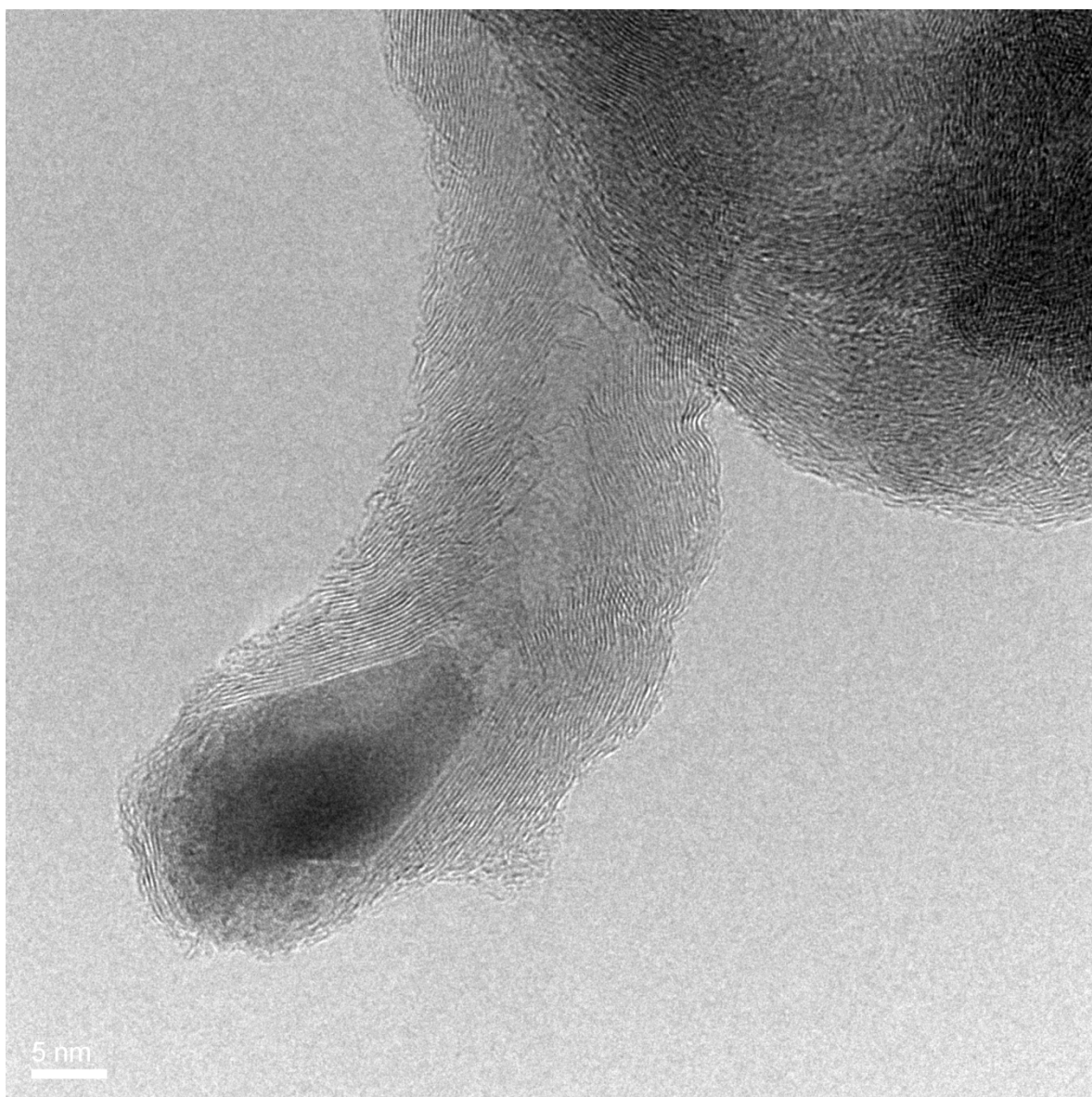


**Figure S6.** Typical high magnification TEM image of the sample prepared with Ni(SA)<sub>2</sub> at 450 °C for 24 hrs.

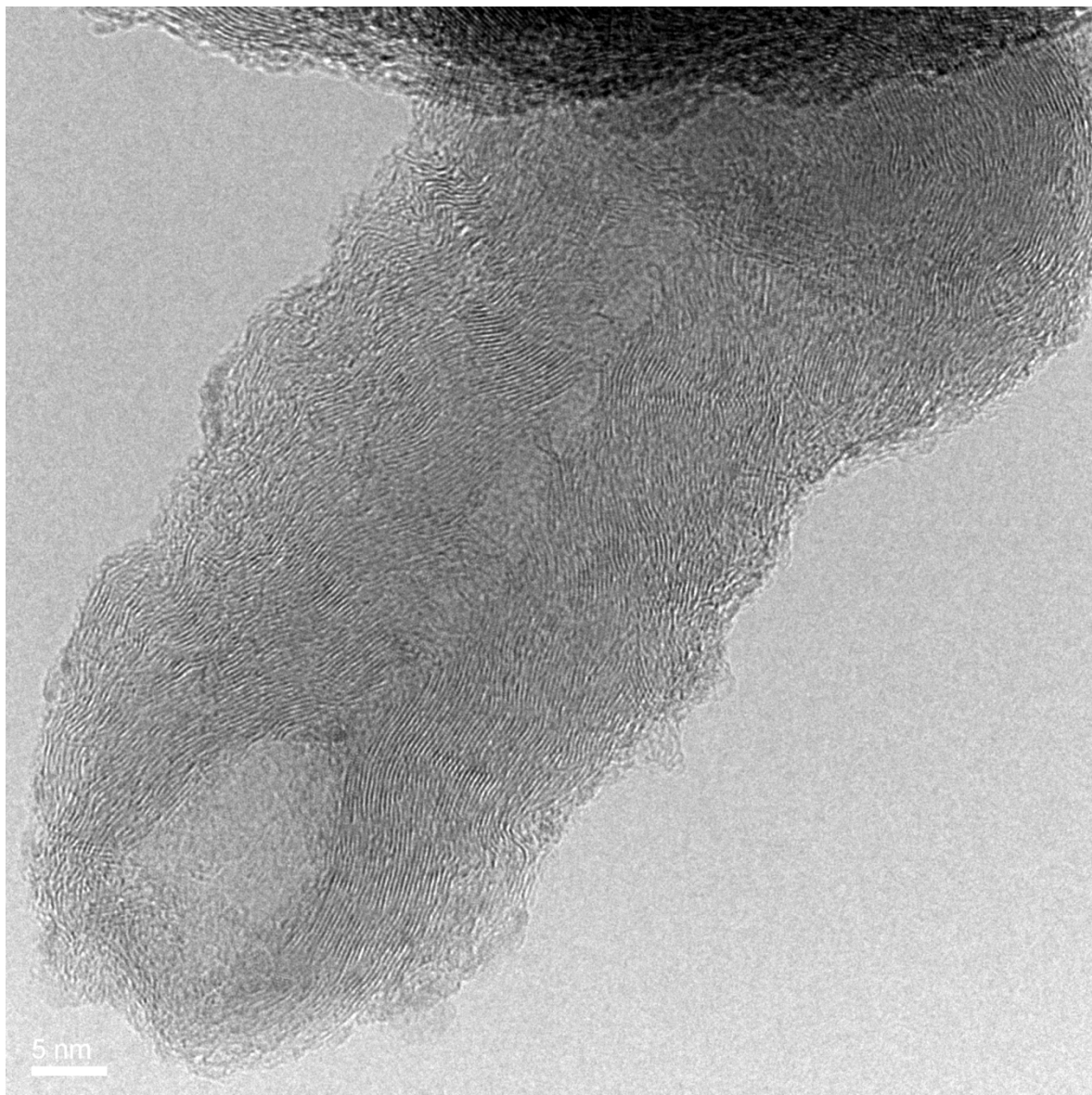


**Figure S7.** Typical high magnification TEM image of the sample prepared with Ni(SA)<sub>2</sub> at 400 °C for 24 hrs.

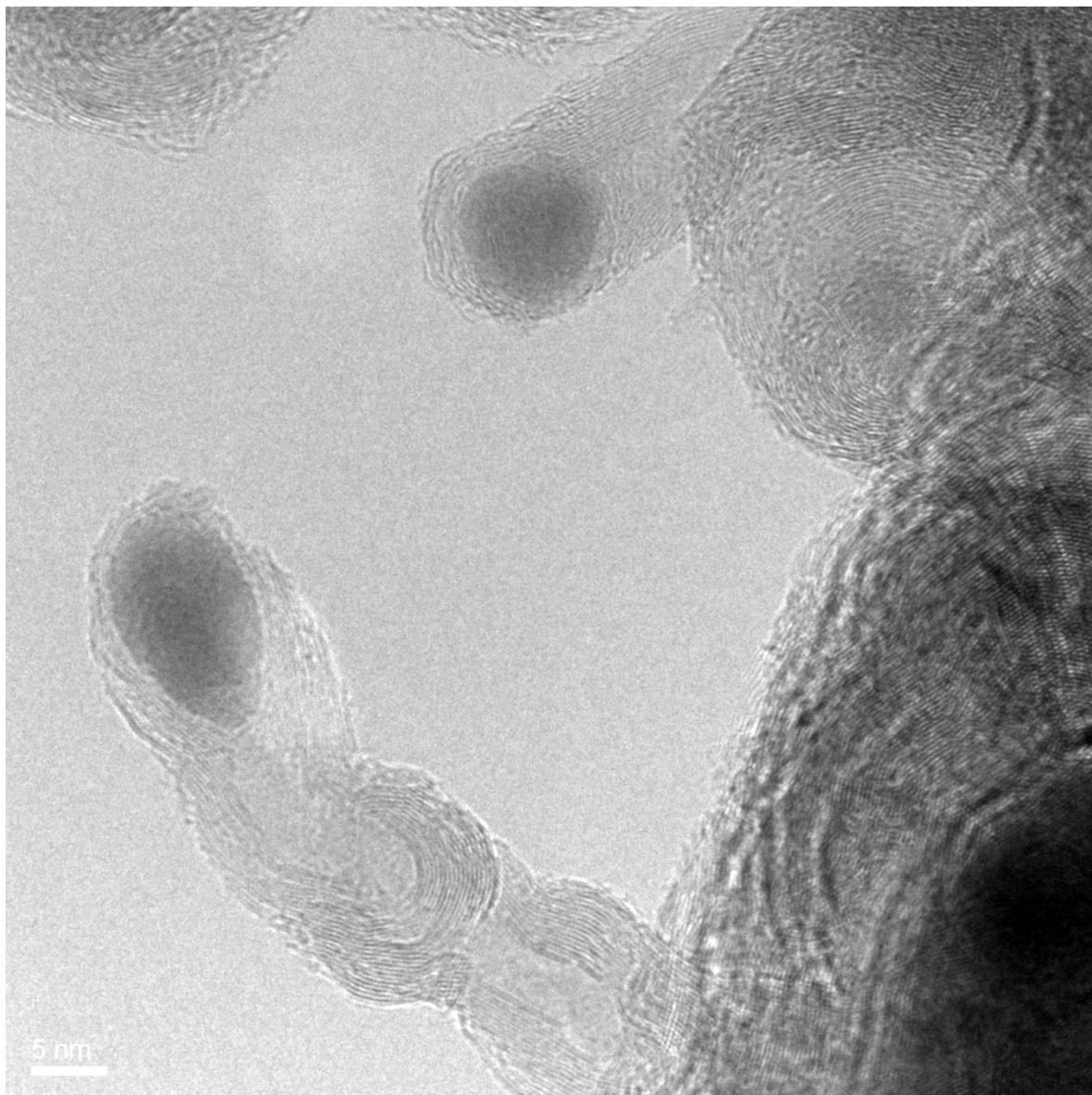


**Figure S8.** Typical high magnification TEM image of the sample prepared with  $\text{Fe(SA)}_3$  at 500 °C for 24 hrs.

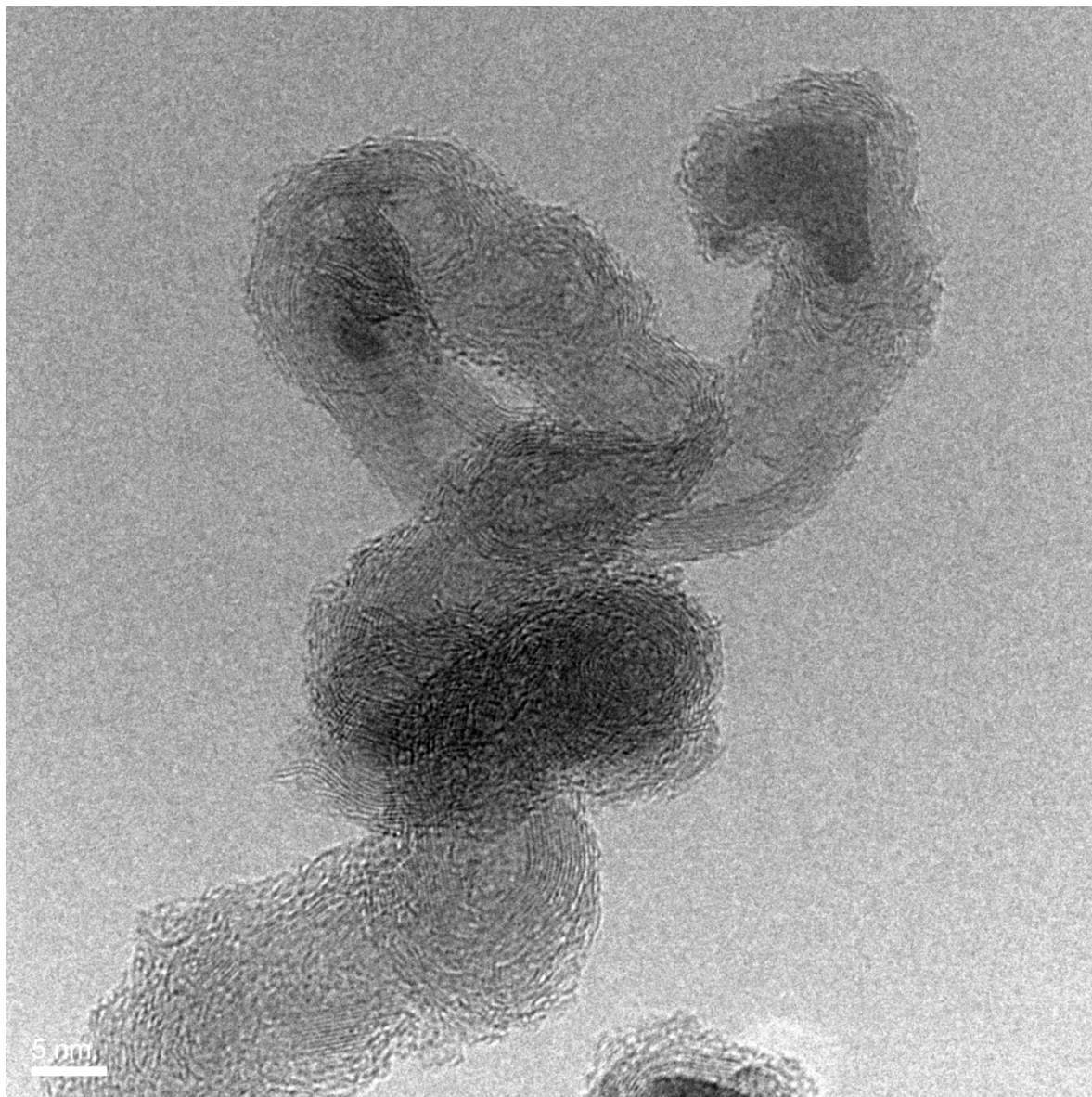


**Figure S9.** Typical high magnification TEM image of the sample prepared with  $\text{Fe(SA)}_3$  at  $450\text{ }^\circ\text{C}$  for 24 hrs.

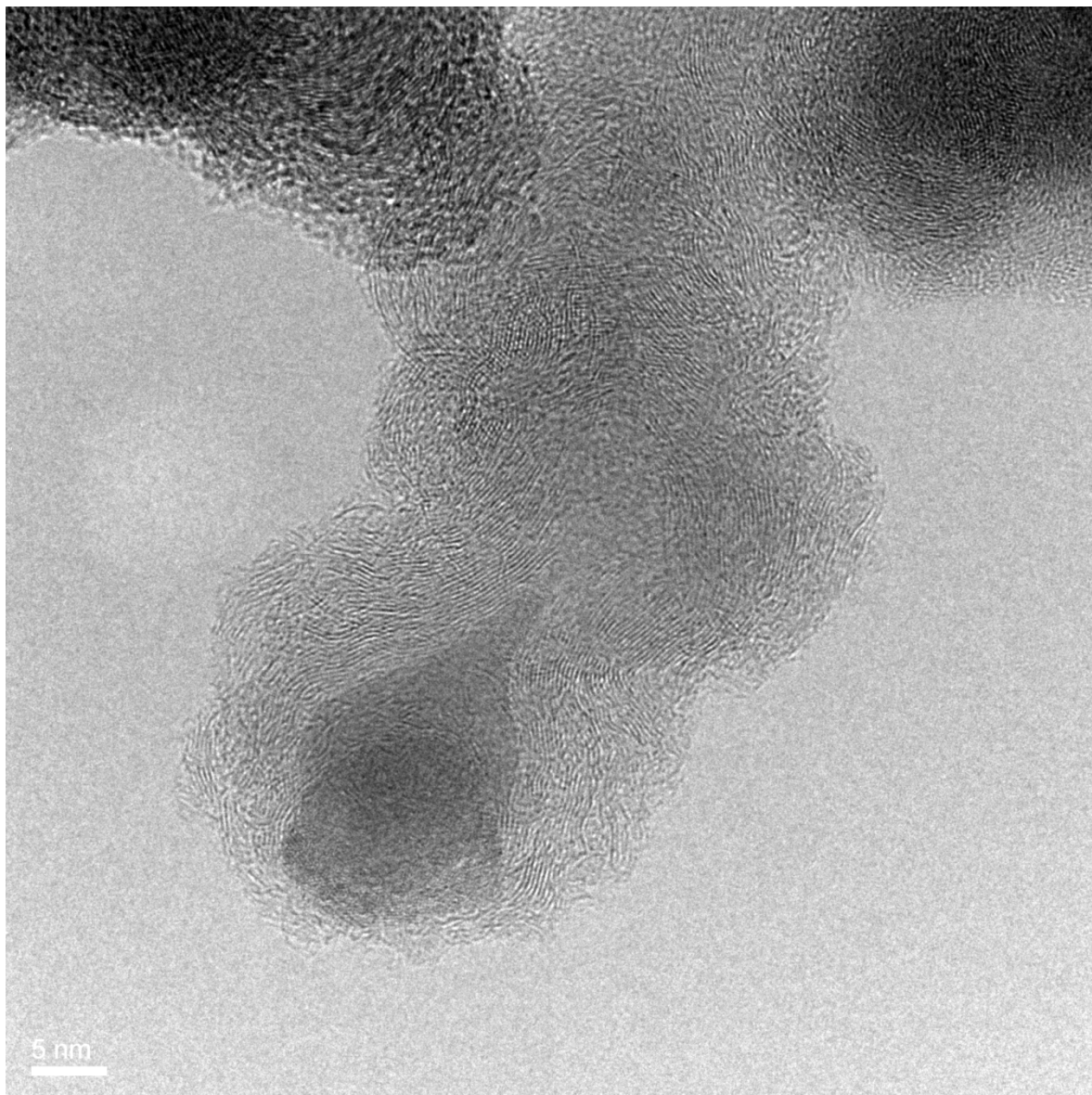


**Figure S10.** Typical high magnification TEM image of the sample prepared with  $\text{Fe}(\text{SA})_3$  at 400 °C for 240 hrs.

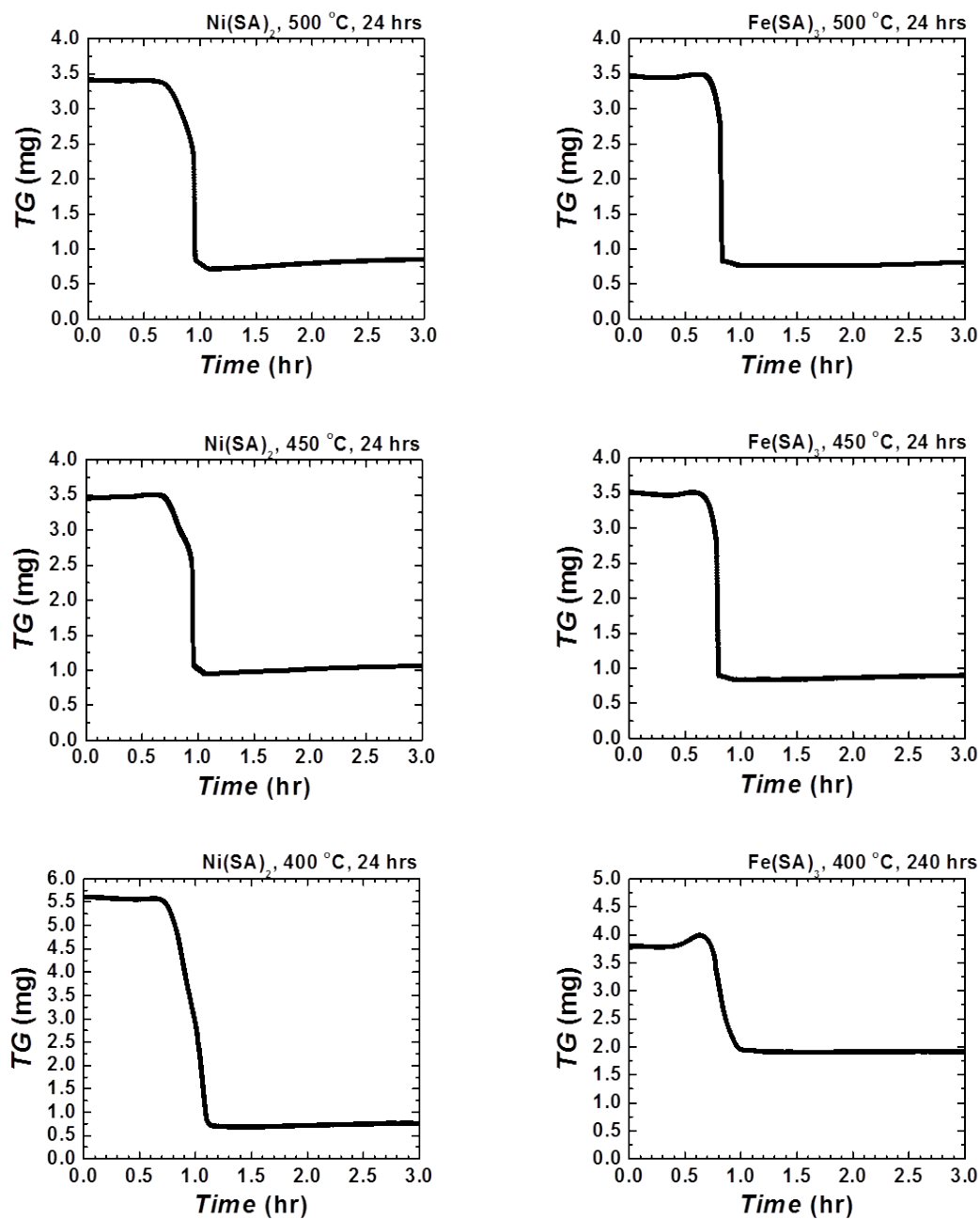


**Figure S11.** TG data. The measurements were performed by heating the sample up to 700 °C (10 °C/min) and kept for 2 hrs under oxygen gas flow (100 mL/min). Weight fraction of the magnetic element (Ni or Fe) in the sample was calculated from the weight of the final oxidized products ( $\alpha$ -Fe<sub>2</sub>O<sub>3</sub> or NiO).

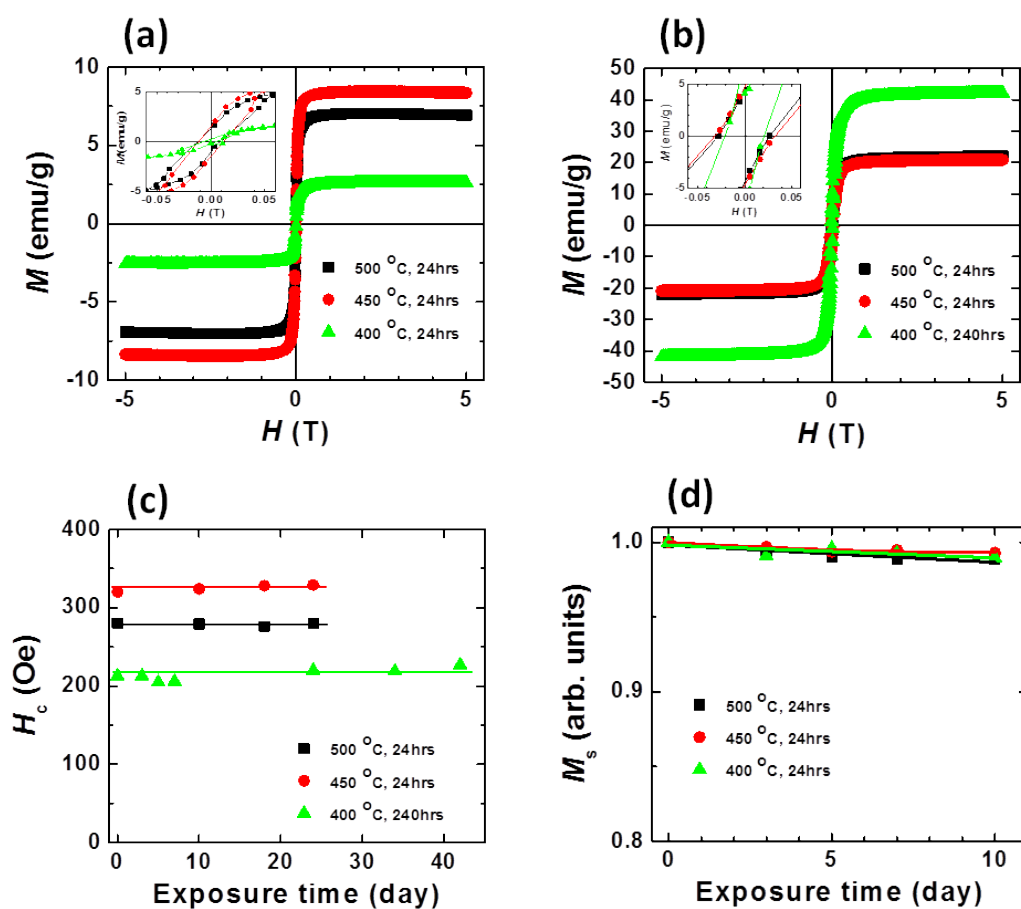
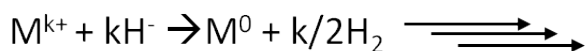


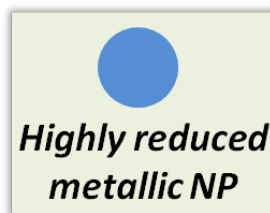
**Figure S12.** Room temperature hysteresis loops of the (a) Ni and (b) Fe NP-loaded MWCNTs. Here,  $M$  is defined as magnetization normalized by the net sample weight. Insets are magnified views of the plots. (c) Time evolution of room temperature coercivity ( $H_c$ ) of the Fe NP-loaded MWCNTs. The linear lines are the guides to eyes. (d) Time evolution of  $M_s$  of the Ni NP-loaded MWCNTs. The as-prepared samples have  $M_s$ s of 6.9, 8.3 and 2.6 emu/g for  $T_r = 500, 450$  and  $400$  °C, respectively. The linear lines are the least squares fittings used to estimate daily decrease in  $M_s(d)$ . For values of  $d$ , see Table S1 in ESI.

### Reactions of metal cations with hydride anions (H<sup>-</sup>)



M: Ni, k = 2

M: Fe, k = 3



### Reactions of stearate with hydride anions (H<sup>-</sup>)

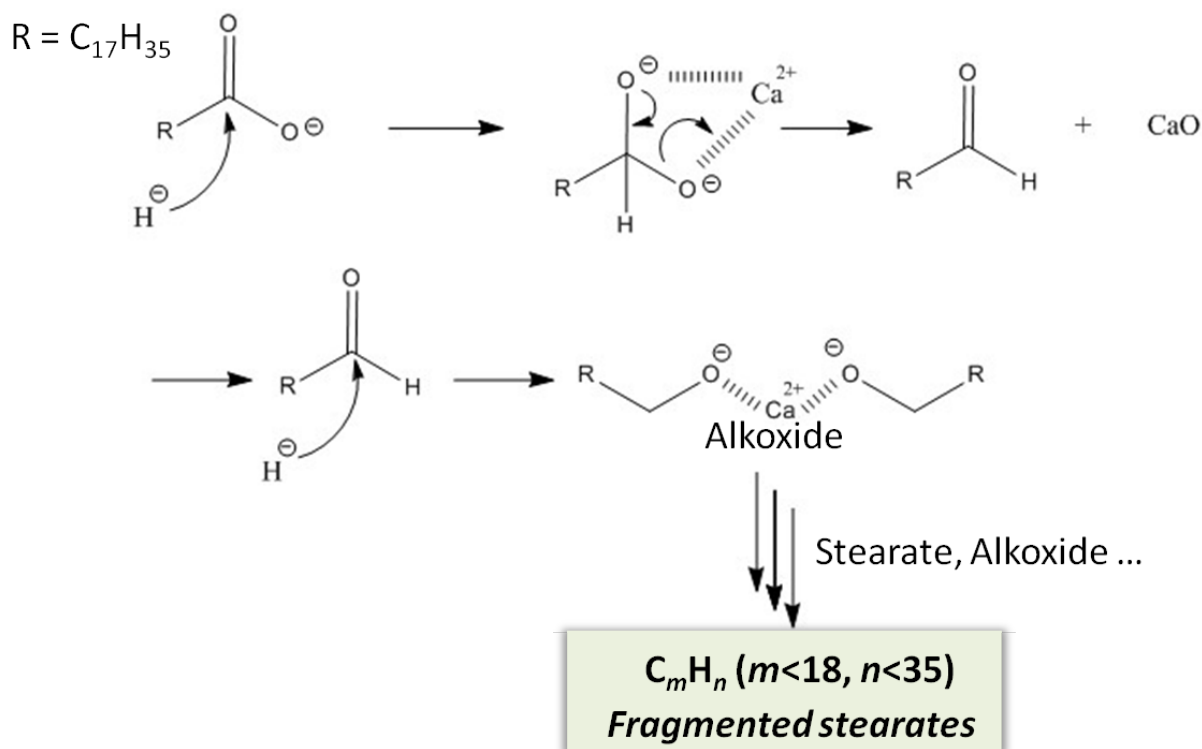


**Figure S13.** Schematic representation of possible mechanisms for dual roles of CaH<sub>2</sub>. Hydride anions (H<sup>-</sup>) from CaH<sub>2</sub> play important roles; Ni<sup>2+</sup> and Fe<sup>3+</sup> are reduced to metallic state via reaction with the hydride anions to form metallic NPs. Thus-formed metallic NPs are highly reduced to have superior catalytic activity<sup>3</sup> due to the very strong reducing ability of CaH<sub>2</sub> at low temperatures<sup>1,2</sup>. On the other hand, the hydride anions may also react with stearate in a similar manner as reactions in solutions to give an alkoxide which are highly reactive toward protons. Because of the high reaction temperatures (> 400 °C) and no other proton sources available in the reaction mixture due to excess CaH<sub>2</sub>, the alkoxide might remove protons from stearate and the alkoxide facilitating their decomposition into fragments. Formation of such fragments was confirmed by the model reaction using stearic acid (see Figure S18 in ESI), although the detailed reaction mechanisms are not clear at present. These data strongly suggest that CaH<sub>2</sub> decomposes stearate into fragments (C<sub>m</sub>H<sub>n</sub>, m < 18, n < 35) which seem to have higher reactivity than stearate.

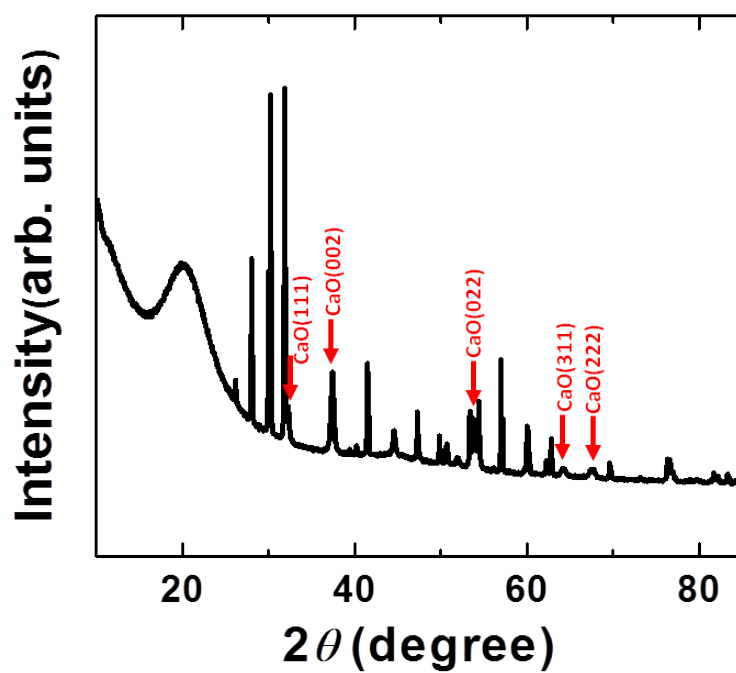


**Figure S14.** Typical XRD pattern of the reaction mixture before washing. The reaction was done with  $\text{Ni}(\text{SA})_2$  at 500 °C for 24 hrs. Formation of CaO is clearly seen.

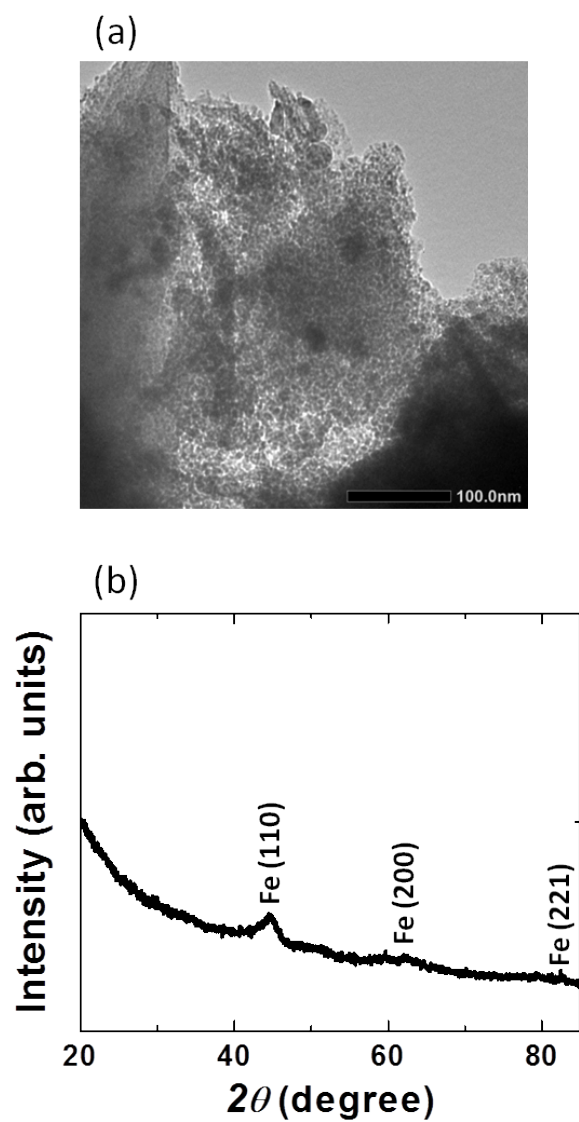


**Figure S15.** (a) TEM image and (b) XRD pattern of the product prepared with Ferrocene at 500 °C for 24 hrs. No MWCNTs as well as graphitic peaks were observed.

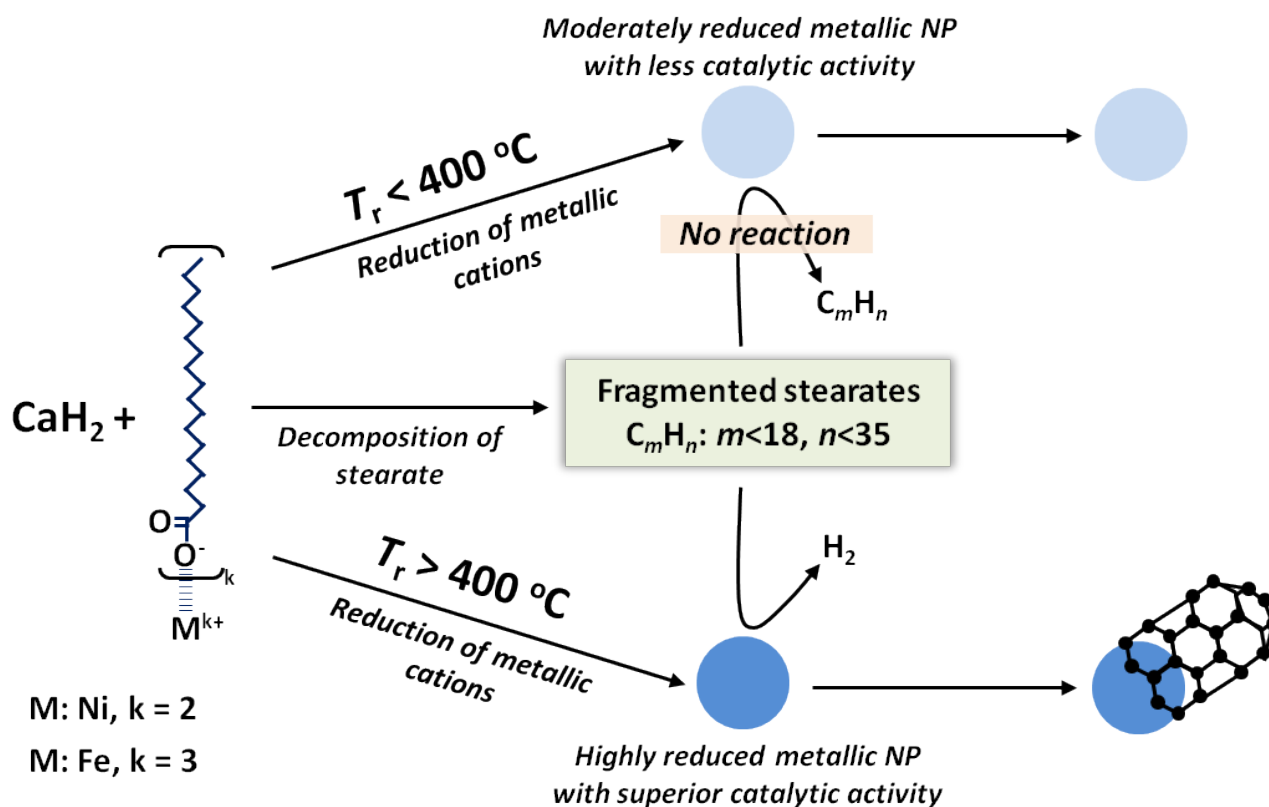
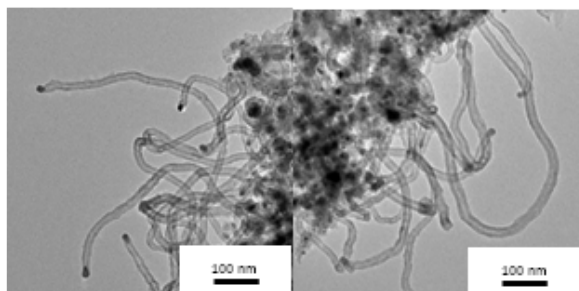
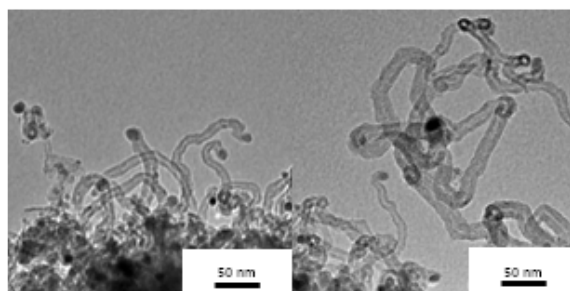


**Figure 16.** Schematic representation of possible reactions with metallic NPs at low temperatures. It has been reported that degree of reduction of the catalyst NPs has strong influences on formation of CNTs at low temperatures<sup>3</sup>.  $CaH_2$  is known to have a very strong reducing ability at low temperatures<sup>1,2</sup>. Therefore, the metallic NPs are highly reduced and are considered to have enough catalytic activity to form MWCNTs even at 400 °C. The actual carbon feedstocks on the metal NPs are the fragments into which  $CaH_2$  decomposes stearate. Decomposition of such fragments to form MWCNTs is considered to be enhanced due to their possible higher reactivity than stearate. This idea is supported by the fact that ferrocene, whose organic ligands (cyclopentadiene) do not react with  $CaH_2$ , formed no MWCNTs even at 500 °C.

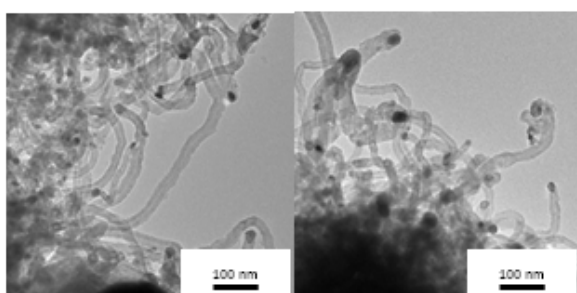
**Ni(SA)<sub>2</sub>, 500 °C, 24 hrs**



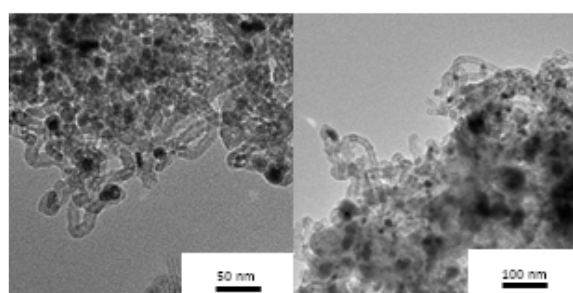
**Fe(SA)<sub>3</sub>, 500 °C, 24 hrs**



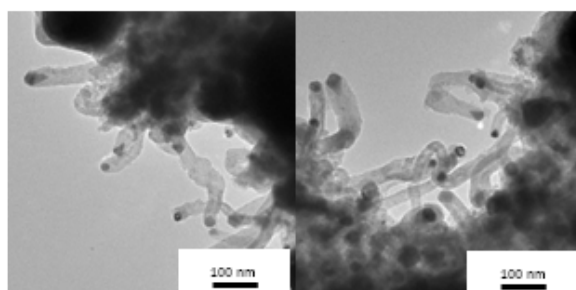
**Ni(SA)<sub>2</sub>, 450 °C, 24 hrs**



**Fe(SA)<sub>3</sub>, 450 °C, 24 hrs**



**Ni(SA)<sub>2</sub>, 400 °C, 24 hrs**



**Fe(SA)<sub>3</sub>, 400 °C, 24 hrs**

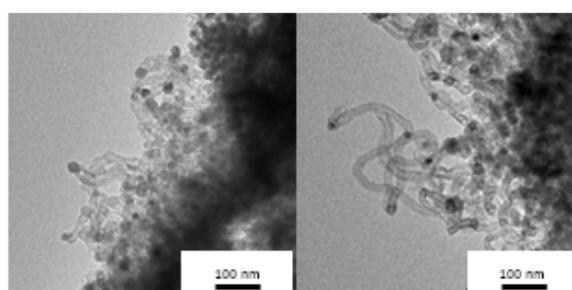


**Figure S17.** Additional TEM images.

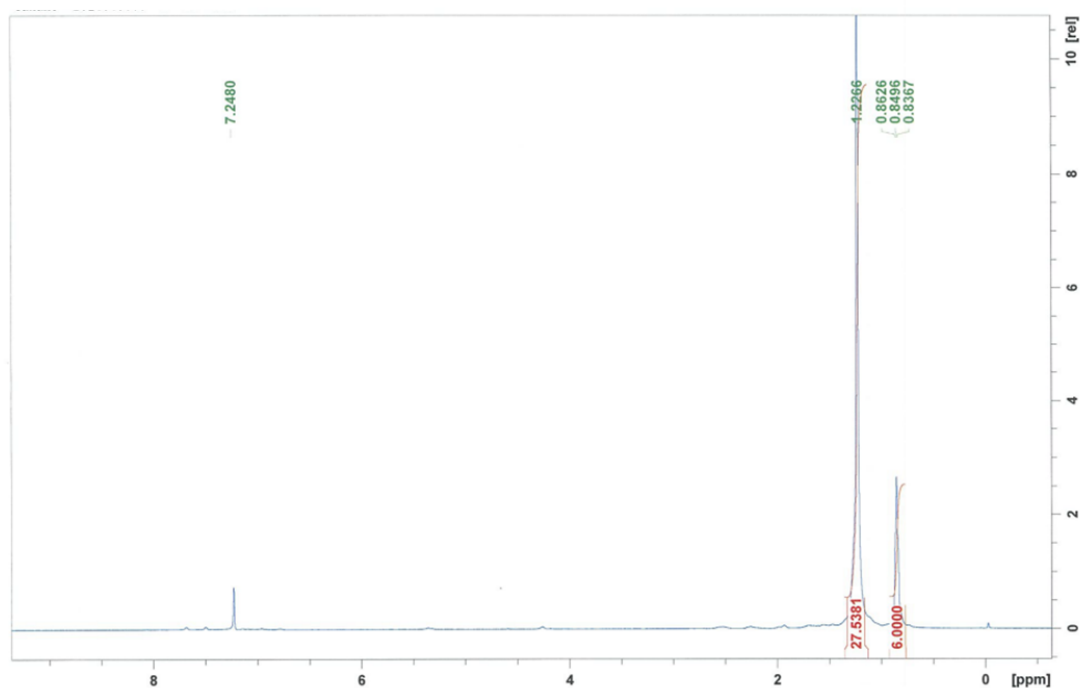


**Figure S18.**  $^1\text{H-NMR}$  spectrum of the crude mixture of  $\text{CaH}_2$  and stearic acid (1/2 in weight) reacted at  $400\text{ }^\circ\text{C}$  for 24 hrs. Strong signals from methyl ( $-\text{CH}_3$ ,  $\delta \sim 0.85\text{ ppm}$ ) and methylene ( $-\text{CH}_2-$ ,  $\delta \sim 1.23\text{ ppm}$ ) protons are observed. Note that a signal appeared around  $\delta \sim 7.3\text{ ppm}$  is from  $\text{CHCl}_3$  involved in  $\text{CDCl}_3$ . The relative intensity ratio ( $I_{\text{CH}_3}/I_{\text{CH}_2}$ ) is 0.2179. This is larger than that expected for octadecane ( $\text{CH}_3-(\text{CH}_2)_{16}-\text{CH}_3$ ,  $I_{\text{CH}_3}/I_{\text{CH}_2} = 0.1875$ ), revealing that  $\text{CaH}_2$  decomposes stearic acid into fragments.

**Table S1. Magnetic properties of the samples at room temperature.**

System	Ni(SA) <sub>2</sub>			Fe(SA) <sub>3</sub>		
$T^a$ (°C)	500	450	400	500	450	400
$M_s^b$ (emu/g-sample)	6.9	8.3	2.6	22.1	20.9	42.0
$M_s^b$ (emu/g-metal)	35	36	29	110	116	111
$H_c^c$ (Oe)	122	113	65	280	320	213
$d^d$ (%)	0.01	0.01	0.01	0.09	0.09	0.11

a) Reacted for 24 hrs except for the case of 400 °C in the Fe(SA)<sub>3</sub> system (240 hrs).

b) Values for the as-prepared samples.

c) Coercivity of the as-prepared samples.

d) Daily decrease in  $M_s$ .

**Calculation of thickness ( $d_{\text{oxide}}$ ) of the surface oxide layer and volume fraction of the metallic core ( $\phi$ ) of the as-prepared Ni NP-loaded samples**

Calculation was done under the following assumptions: the oxide layer is NiO with saturation magnetization of 0 emu/g and specific gravity of 6.67. The particle shape is spherical with a diameter of  $D_{\text{NP}}$ . The core is fcc-Ni with an ideal saturation magnetization of 55 emu/g<sup>4</sup> and specific gravity of 6.67.

**Table S2. Structural parameters of the as-prepared Ni NP-loaded samples**

system	Ni(SA) <sub>2</sub>		
$T^{\text{a}}$ (°C)	500 °C	450 °C	400 °C
$D_{\text{NP}}^{\text{b}}$ (nm)	16 ± 7	20 ± 6	26 ± 10
$\sigma^{\text{c}}$	0.19	0.24	0.09
$d_{\text{oxide}}$ (nm)	1.4	1.6	3
$\phi$	0.57	0.59	0.46

a) Reacted for 24 hrs.

b) Diameter of the metallic NPs (mean ± standard deviation) estimated on the average of > 100 particles in the TEM images.

c) Weight fraction of the magnetic element estimated by thermogravimetric analysis.

## References for ESI

1. S. Yamamoto, G. Ruwan, Y. Tamada, K. Kohara, Y. Kusano, T. Sasano, K. Ohno, Y. Tsujii, H. Kageyama, T. Ono, and M. Takano, *Chem. Mater.*, 2011, **23**, 1564.
2. L. Seinberg, S. Yamamoto, R. Gallage, M. Tsujimoto, Y. Kobayashi, S. Isoda, M. Takano and H. Kageyama, *Chem. Comm.*, 2012, **48**, 8237.
3. E. Mora, J. M. Pigos, F. Ding, B. I. Yakobson and A. R. Harutyunyan, *J. Am. Chem. Soc.*, 2008, **130**, 11840.
4. J. H. Hwang, V. P. Dravid, M. H. Teng, J. J. Host, B. R. Elliott, D. L. Johnson, and T. O. Mason, *J. Mater. Res.* 1997, **12**, 1076.